



RESEARCH ARTICLE

10.1029/2019JA027592

A Possible Explanation of Interhemispheric Asymmetry of Equatorial Plasma Bubbles in Airglow Images

Dustin A. Hickey¹ , Sukanta Sau² , V. L. Narayanan³ , and S. Gurubaran²

¹National Research Council Postdoctoral Research Associate, Space Science Division, U.S. Naval Research Laboratory, Washington, DC, USA, ²Indian Institute of Geomagnetism, Navi Mumbai, India, ³Department of Physics and Technology, UiT-The Arctic University of Norway, Tromsø, Norway

Key Points:

- An interhemispheric asymmetry observed in the tilt of EPBs during a severely disturbed period has been re-analyzed here
- The asymmetry is attributed to a variation in airglow emission altitude within the field of view of an all-sky imager
- Modeling results and nearby measurements provide evidence for this variation

Correspondence to:

D. A. Hickey,
dustin.hickey.ctr@nrl.navy.mil

Citation:

Hickey, D. A., Sau, S., Narayanan, V. L., & Gurubaran, S. (2020). A possible explanation of interhemispheric asymmetry of equatorial plasma bubbles in airglow images. *Journal of Geophysical Research: Space Physics*, 125, e2019JA027592. <https://doi.org/10.1029/2019JA027592>

Received 30 OCT 2019

Accepted 19 FEB 2020

Accepted article online 28 FEB 2020

Abstract Equatorial plasma bubbles resulting from equatorial spread F are well known to be aligned along the Earth's geomagnetic fields. During the geomagnetic storm on 17 March 2015, all-sky airglow observations from Tirunelveli (8.7°N, 77.8°E, 1.7°N dip latitude) showed an apparent interhemispheric asymmetry in the tilt of the equatorial plasma bubbles. In this work we further investigate this case and provide a possible explanation for the asymmetry. We suggest that a variation in the altitude of the airglow layer across the image can cause the observed asymmetry. If the airglow layer is at a higher altitude in the northern portion of the image, then this would explain the observed asymmetry. This variation in the airglow layer can be caused by a variation in the height of the ionosphere. We show through modeling and ionosonde observations that it is likely that there is a variation in the airglow altitude within the field of view of the images on this night.

1. Introduction

Equatorial spread F (ESF) is a common nighttime occurrence in the low-latitude ionosphere. Although ESF has been studied for decades, its spatial and temporal variability are not well understood. ESF refers to nighttime equatorial plasma bubbles (EPBs) and their associated irregularities that result from the Generalized Rayleigh-Taylor Instability. EPBs generated by ESF are a field-aligned process which means that the large-scale plasma depletions occur all along the magnetic field lines (Farley Jr. 1960; Otsuka et al., 2002). As a result, the topside of the EPBs over the magnetic equator is mapped along geomagnetic field lines to the bottomside ionosphere away from the magnetic equator.

There are many different instruments that are used to detect and analyze ESF. Ionosondes can determine the presence of ESF but are not able to observe its morphology (e.g., Abdu et al., 2000). Coherent backscatter radars are able to detect the small-scale irregularities associated with EPBs and can determine the altitudinal and temporal extent of these small-scale irregularities (e.g., Hysell & Burcham, 2002). Observations using the Global Navigation Satellite System can also show the presence and strength of small- and medium-scale irregularities at a given location and altitude (e.g., Kelley et al., 1996). All-sky airglow imagers (ASIs) are able to detect the 2-D longitude-latitude structure of EPBs at a given altitude (Mendillo & Baumgardner, 1982; Weber et al., 1983). At the magnetic equator, images from ASIs show the bottomside structure of EPBs and away from the magnetic equator they show topside plumes since the flux tubes trace to the topside over the magnetic equator (e.g., Weber et al., 1978).

Geomagnetic storms are known to have an impact on the formation of EPBs and can either enhance or suppress their development depending on the local time of occurrence (Martinis et al., 2005; Tulasi Ram et al., 2008). The St. Patrick's Day geomagnetic storm of 2015 (17 March) is a particularly well studied storm and the largest one in solar cycle 24. Recently, Sau et al. (2017) presented airglow observations over the Indian low-latitude sector during the St. Patrick Day's storm of 2015. On 17 March 2015, EPBs were observed with two ASIs over India. Between 16 and 18 UT on this day, the EPBs show a westward tilt to north of the magnetic equator, which is fairly typical for these features (Weber et al., 1980). However, at conjugate latitudes to the south of the magnetic equator, no significant tilt is observed in the EPBs meaning that the features are asymmetric with respect to the magnetic equator. These observations appear to be inconsistent with the field-aligned nature of ESF.

©2020. The Authors.

This is an open access article under the terms of the Creative Commons Attribution-NonCommercial-NoDerivs License, which permits use and distribution in any medium, provided the original work is properly cited, the use is non-commercial and no modifications or adaptations are made.

In this paper, we further analyze the observations reported in Sau et al. (2017) along with ionosonde measurements carried out close to the magnetic equator and at a low-latitude station in the Indian longitude sector. In addition, we have also utilized outputs from a few models, such as the International Reference Ionosphere (IRI-2016) (Bilitza et al., 2017), the Naval Research Laboratory Mass Spectrometer Incoherent Scatter Radar model that extends to the exobase (NRLMSISE-00), and Sami2 is Another Model of the Ionosphere (SAMI2) to understand effects of geomagnetic storm on the equatorial electrodynamics. In this work, we provide an explanation for the asymmetry observed in the tilt of the EPBs in a way that is consistent with their field-aligned nature by taking into account the possible altitude variations of the airglow emission layer within the field of view (FoV) covered by an imager. The analysis made here has important implications for two-dimensional horizontal spatial observations of upper atmospheric parameters in general. For example, GPS TEC maps are generally retrieved assuming a fixed height of ionospheric pierce points but our results indicate that there may be significant variation of these altitudes.

2. Instruments and Methods

In this paper, we focus on images obtained from the ASI installed at Tirunelveli (8.7°N, 77.8°E, 1.7°N dip latitude). This imager contains a filter at 630.0 nm (bandwidth ~ 2 nm) that is used to observe emission from excited atomic oxygen (OI) in the thermosphere. OI 630.0 nm emissions are well suited for observing the large-scale structure of EPBs. Regions of low plasma density have less emission intensity compared to regions of high plasma density. Consequently, EPBs are generally observed as dark regions against the relatively bright background. The 630.0 nm emission comes from a relatively small altitude range about 50 km below the peak of the *F* region (Abalde et al., 2004; Mendillo & Baumgardner, 1982). The typical peak altitude of emission is about 250 km. Both this altitude and the intensity of 630.0 nm emission vary depending on the altitude and density of the background ionosphere and thermosphere. As a result, the peak height and intensity of emission can vary within the FoV of an ASI and throughout the night. As an example, at the magnetic equator the height and intensity of emission can change drastically as the ionosphere rises up early in the night during the prereversal enhancement (PRE) and then moves back down later in the night (Hickey et al., 2018).

For an accurate analysis of EPBs in OI 630.0 nm images, an altitude of emission must be determined. The altitude of emission will impact the size and shape of the features within the FoV. To fully determine the altitude of emission, height profiles of ion density, ion temperature, electron density, electron temperature, neutral density, and neutral temperature are needed. In most situations none or very few of these profiles are available. A reasonable estimation of airglow altitude can be calculated using ionospheric profiles from IRI-2016 (Bilitza et al., 2017) and thermospheric profiles from NRLMSISE-00 (Picone et al., 2002). For ease of image analysis a constant airglow altitude is often assumed for the entire image (e.g., Martinis et al., 2003), as was done in Sau et al. (2017). However, the airglow images of thermospheric emissions cover a large area over 1.2×10^6 km² at 250 km. The assumption that the altitude of the emission layer is constant is not always valid, especially near the magnetic equator and the crests of equatorial ionization anomaly since the height of the ionosphere in these regions can vary significantly throughout the FoV of the imager (Rama Rao et al., 2006).

Variations in the height of the ionosphere result in a variation in the height of the airglow layer and can have a few effects on the analysis of the image. Changing the height of the assumed airglow emission for a given image will change the size and extent of the features within the image (Abalde et al., 2004). If a 630.0 nm image is unwrapped at an altitude higher than the typically assumed 250 km, then the features, such as EPBs, will be wider and the images will extend over a larger range of magnetic latitudes as well. If a lower altitude is used, then the EPB features will be thinner and will cover a smaller range of magnetic latitudes. The height of the airglow layer will also impact which magnetic field lines cross through the image and thus the magnetic apex altitudes they reach.

In this paper we use both model-based calculations and observations to have a better estimate of the airglow altitude in comparison to the assumed altitude of 250 km that was used in Sau et al. (2017). A reasonable estimation of airglow altitude can be calculated using ionospheric profiles from IRI-2016 (Bilitza et al., 2017) and thermospheric profiles from NRLMSISE-00 (Picone et al., 2002). We have calculated the volume emission rate (VER) of 630 nm emission with the help of the VER equation described in Colerico et al. (2006),

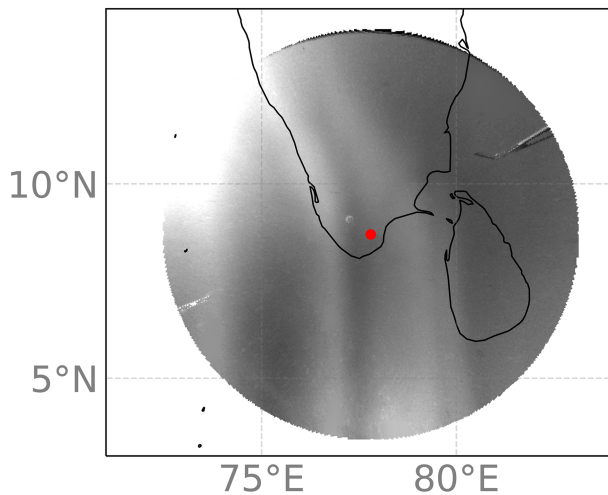


Figure 1. An airglow image at 630.0 nm from Tirunveli on 17 March 2015 at 17:06 UT. It has been unwrapped at an altitude of 250 km.

Sau et al. (2018), and Sobral et al. (1993). The VER is calculated using altitude profiles of electron density, electron temperature, ion temperature, O_2 density, N_2 density, O density, and neutral temperature. The chemical reactions that produce 630.0 nm emission are used to do the calculation. The altitude where the VER of 630 nm emission attains maximum is considered as the peak airglow emission altitude. The peak airglow emission altitude is calculated based on the method described in the previous works cited here. The electron density profile, electron, and ion temperature are taken from IRI-2016, while densities of the neutral thermospheric constituents and neutral temperature are taken from NRLMSISE-00 as inputs into the airglow calculation. The constant values and equations for the reaction rate coefficients used in the calculation are taken from Sobral et al. (1993).

The asymmetry of EPB tilts between the conjugate points observed by Sau et al. (2017) is shown in Figure 1. Note that the asymmetry in the tilt of the EPBs is observed in the approximately north-south direction since the magnetic declination is small in the Indian sector. In order to examine whether any airglow layer altitude variation could have caused the asymmetry, we calculate the altitude of the airglow layer at different latitudes. Since the time when asymmetry occurred is ~ 3 hr after sunset,

we assume that there is minimal variation in the altitude of airglow layer over the relatively thin longitudinal width of the EPBs. To further investigate variations in airglow altitudes, SAMI2 is utilized in this work (Huba et al., 2000). SAMI2 is a 2-D (in altitude and latitude coordinates), low-latitude model of the ionosphere.

Finally, we use observations from two identical Canadian Advanced Digital Ionosonde (CADI) to better determine the height of the ionosphere over Southern India during the geomagnetic storm of 17 March 2015. One CADI is colocated with the imager at Tirunelveli, and the other one is situated at a low-latitude station at Hyderabad (17.4°N lat, 78.5°E lon, 11.7°N dip latitude). The CADI at Hyderabad is located just outside the FoV of the ASI, and it is approximately 960 km north of Tirunelveli. On 17 March 2015, ionograms were obtained at a cadence of 10 min both at Tirunelveli and Hyderabad. Technical details of the CADIs in operation in the Indian region are briefly discussed in Narayanan et al. (2014).

3. Hypothesis for Observed Asymmetry

Sau et al. (2017) showed that there is a clear north-south asymmetry in the tilt of the plasma bubbles observed on 17 March 2015. The depletions to the north of the magnetic equator are tilted to the west, and at the same time the depletions to the south show no tilt. We propose that a variation in the altitude of the airglow layer across the FoV of the imager can lead to this apparent asymmetry.

As discussed earlier, an altitude of 250 km is often assumed to be the peak altitude of the 630.0 nm emission for the whole duration of the night. When 250 km is not assumed, then the typical process is to calculate the emission profile using empirical models and then use the peak of the emission as the altitude for analysis. This altitude is assumed to be constant throughout the FoV of the imager. Multiple measurements of ionospheric density profiles at different locations within the FoV of the imager would be required to determine the variation of emission altitude throughout the FoV. Since such measurements are not available, we use empirical and physics-based models to investigate this variation.

IRI-2016 and NRLMSISE-00 are initially used to calculate the peak altitude of 630.0 nm emission at the location of the imager. These models are run throughout the night for the same date as the images, 17 March 2015, and use the same geomagnetic and solar conditions from this day. At the center of the image at 16:48 UT (22:18 IST), the calculated peak emission altitude is 258 km. This time corresponds to when the tilt of the EPBs started increasing in the northern half of the images. The obtained peak emission altitude is close to the assumed 250 km used in Figure 1 and Sau et al. (2017). The two empirical models are then used to calculate the airglow altitude throughout the night. Figure 2 shows the change in the 630.0 nm airglow altitude throughout the night. This figure shows that at the location of this ASI, using IRI-2016 and NRLMSISE-00, the airglow emission altitude varies by 35 km throughout the night. This shows that a significant variation in the altitude occurs throughout the night and indicates that using 250 km for the

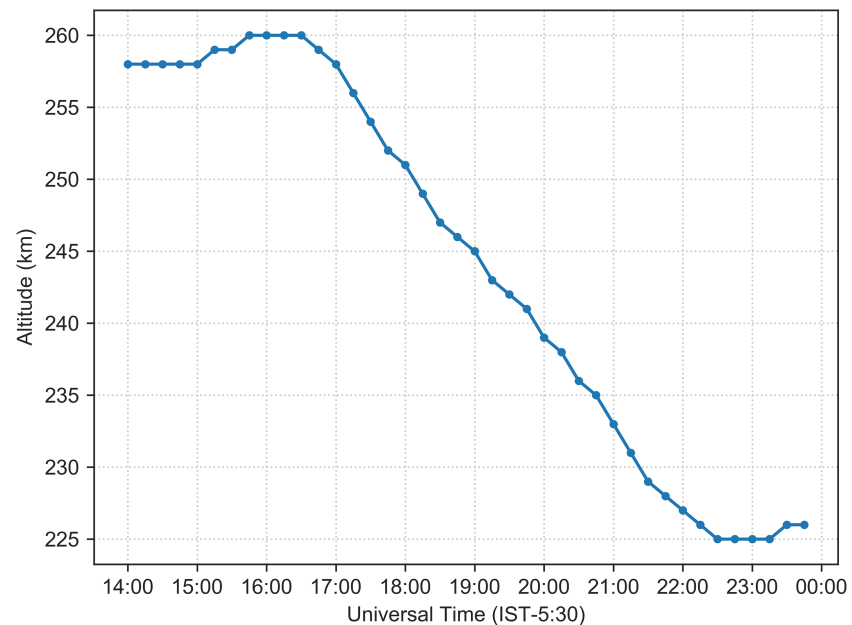


Figure 2. Peak emission altitude of 630.0 nm emission throughout the night on 17 March 2015. The inputs for this calculation are from IRI-2016 and NRLMSISE-00.

whole night is not the best approach. A variation in altitude of 35 km can change the size of the features in the image by around 12.5%. The variation at this site is mostly due to the rising of the ionosphere early in the night as a result of the PRE and then moving back down after the end of the PRE.

In addition to calculating the airglow altitude at the center of the image with these empirical models, we also calculate the airglow altitude as a function of latitude on a constant longitude through the center of the image. The altitude was calculated from a latitude range of 4°N to 14°N. The airglow altitude only varied by about 3 km throughout the image when the calculation is done using IRI-2016 and NRLMSISE-00. Although the airglow calculation using empirical models does not show significant variation of airglow altitude in the region of the image, we do not expect these models to reproduce results for a given day since they are climatological. Since IRI-2016 is empirical, it is not expected to reproduce the ionospheric variability on scales of hundreds of kilometers during a strong geomagnetic storm. Additionally, NRLMSISE-00 is not able to reproduce small-scale variations less than 15° (Hedin et al., 1977; Picone et al., 2002). These empirical models are expected to better capture the temporal variation shown in Figure 2 compared to the small-scale spatial variation. This means that even though the empirical models do not show a significant variation in airglow altitude with latitude, this is not necessarily indicative of reality. To better understand the variation in the airglow altitude, SAMI2 is used for a simple analysis.

SAMI2 is a physics-based model of the ionosphere that is run using empirical models of the neutral atmosphere and winds as inputs. Using a physics-based model allows us to investigate how the ionosphere varies on smaller scales than can be done with an empirical model of the ionosphere. SAMI2 is used here to do a simple analysis to explore what sources have the ability to impact airglow altitude rather than to find the absolute airglow altitude on the night of observation. We use a grid of 200 × 201, the number of grid points transverse to and along the magnetic field, and have the height span from 90 to 2,000 km. This results in the model covering from 18°S to 35°N in latitude at the longitude of the ASI. We input the date and run the model for 48 hr. The first 24 hr is disregarded to allow the model to stabilize. We are also able to change the geomagnetic conditions of the model by changing ap index value. First, we run the model with $ap = 0$ for quiet conditions. Then we run the model for $ap = 180$ to represent the geomagnetic activity that was occurring on 17 March 2015. We then use the outputs to calculate the airglow altitude as a function of latitude. Figure 3 shows the latitudinal variation of the airglow height during quiet time conditions (blue) and geomagnetically active conditions (orange) on 17 March 2015 at 18:14 UT. Even during quiet time there is a variation in altitude of the peak emission over 10° of latitude. From this we see that the variation between

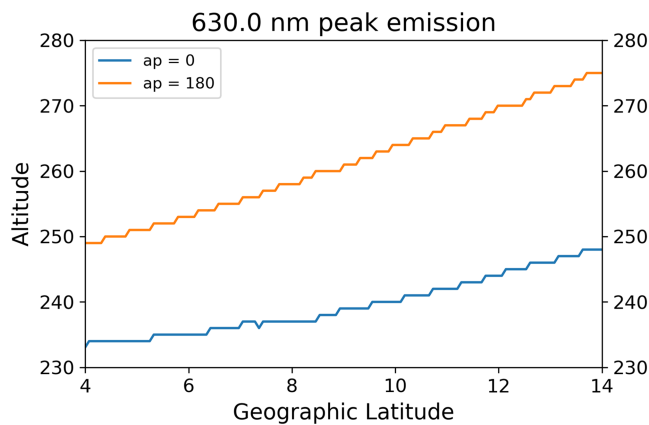


Figure 3. Peak emission altitude of 630.0 nm at 18:14 UT on 17 March 2015 at latitudes across the image. These altitudes were computed using outputs from SAMI2. The two lines show the emission altitude for two different geomagnetic conditions. The blue line shows the results with $ap = 0$ and the orange line with $ap = 180$.

4°N and 14°N latitudes increases from ~ 15 km during quiet times to ~ 25 km during disturbed time. This is very different from the results obtained from the calculation using IRI-2016 and NRLMSISE-00. An analysis of the wind output of the model indicates that the increased altitude variation during geomagnetically active times is due to an increased southward meridional wind. This wind will drag the plasma, causing it to move upward in regions north of the magnetic equator. The SAMI2 results indicate that it is reasonable to expect a variation of airglow altitude over 10° of latitude in this region of India and that during a geomagnetic storm, mainly due to disturbance winds, this variation can be increased.

Next we analyze the image shown in Figure 1 to see how a variation in airglow altitude affects the interpretation of the images. We use this one image from 17:06 UT for all of the analysis here. Generally, ASI images are assumed to be at the same altitude throughout the FoV. Under this assumption, EPBs that are flux tube aligned will be mapped along the field lines to both the hemispheres and should appear like mirror images with the magnetic equator as the reflection point. If the airglow layer

is not at the same altitude throughout the image, then this will cause variations in how the EPB features are observed in the conjugate locations. As we have already discussed, the observed shape of EPBs will be impacted by the actual airglow layer altitudes. The airglow images show how a cross section of the depletions appears at the altitude of the airglow layer. The magnetic field lines are curved such that a slice through the depletion at 250 km will be different from one through the depletion at 300 km. Figure 1 shows the image at a constant altitude of 250 km throughout the entire FoV. To investigate how different airglow altitudes will affect the asymmetry of the EPBs, the data from this time are first unwrapped at additional altitudes of 275 and 300 km. The background ionospheric and thermospheric measurements do not exist between the center of the image and the edges of the image for us to calculate accurate airglow altitudes for the rest of the image. These images at multiple airglow altitudes are used to see how a variation in altitude throughout the image can affect the asymmetry observed in the EPB structure.

The data at 17:06 UT used in Figure 1 are split into two parts to create an image that has a different airglow altitude in the northern part of the image than in the southern part. In order to determine how the altitude affects the asymmetry, we take the northern portion of the image and determine the location of every pixel in that part of the image. In the first part of the analysis we define the northern part of the image to be everything above 7.7°N , which is approximately the location of the magnetic equator. After that, we split the image at 9.6°N , about where the EPB begins tilting to the west. We then calculate the magnetic conjugate location of each pixel. A new image is then created with each pixel now placed at its conjugate location. This analysis is done using apexpy (van der Meeren et al., 2018), a Python wrapper for the Apex fortran library from Emmert et al. (2010), that converts between different magnetic coordinates described in Richmond (1995). The images at Tirunelveli include regions from both north and south of the magnetic equator. If the airglow layer is at the same altitude throughout the image, then a projection of a portion of the image along the magnetic field lines to the opposite hemisphere should produce the same size, shape, and position of the ESF depletions in both the hemispheres. Instead, an asymmetry is observed in the images on 17 March 2015 and that leads us to the hypothesis that the airglow layer is not at the same altitude throughout the FoV.

The first analysis done using this conjugate projection shows how the southern half of the 17:06 UT image should look as a field line mapping of the northern half. The northern half of the image that is used for the projection is everything above 7.7°N geographic latitude. Figure 4 shows this analysis where the top half of the image is at 300 km and then every point is traced along the magnetic field lines and projected in the Southern Hemisphere at 300 km as well. There is a gap between the two parts because the magnetic equator does not exactly follow the line of geographic latitude that was used to split the image. This figure shows what the bottom half of the image should look like if the entire region had the same airglow altitude. The southern half of Figure 4 is quite different compared to the southern half of Figure 1.

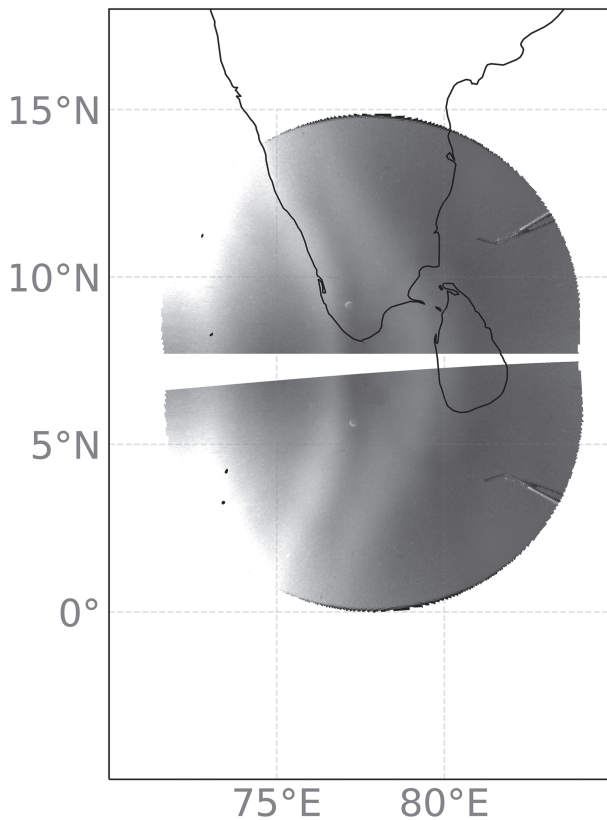


Figure 4. An image from the Tirunelveli ASI on 17 March 2015 at 17:06 UT, the same time as Figure 1. Only the northern portion of the image is shown here, unwrapped at an altitude of 300 km. The northern portion is then traced along magnetic field lines and projected into the Southern Hemisphere.

The next step in this analysis is to determine how a variation in altitude affects the projection. Again, the data at 17:06 UT are split into a northern portion and a southern portion along 7°N geographic latitude. The top half of the image is unwrapped at an altitude of 300 km, and the bottom half of the image is unwrapped at an altitude of 250 km. In reality there would be a continuous transition between the two altitudes but this approach is used for simplicity to illustrate the point, even though it creates a discontinuity between the two portions. The image is split using the same latitude at each altitude. Since it is the latitude that is used and not a constant angle from zenith, there is a small region of overlap at the split location. This results in data at 250 km being covered by data at 300 km. This region is only about 0.2° of latitude and does not impact our results. Additionally, every pixel in the top half of the image is traced along magnetic field lines and projected in the Southern Hemisphere at an altitude of 250 km. This tracing is done from 300 to 250 km in contrast to the tracing from 300 to 300 km that was done in Figure 4. Figure 5 shows all three parts, the northern portion of the image unwrapped at 300 km, the southern portion of the image unwrapped at 250 km, and the field line traced projection in the southern magnetic hemisphere. When the northern half of the image is traced from 300 to 250 km in the Southern Hemisphere, the projection ends up outside the FoV of imager. This is because the higher altitude of the airglow layer would intersect a different part of the ESF depletion, a part that corresponds to a higher apex altitude. From this analysis we can conclude that if the northern portion of the image is at a higher altitude than the southern portion of the image, an asymmetry in the image can be observed because the conjugate location of the northern portion is outside the FoV of the imager.

There has not been much work on the variation of ionosphere altitude within an area covered by the FoV of the imager, about 1.2×10^6 km². Most instruments that can measure the height of the ionosphere are located farther apart than the distance covered in the images. As a result, it is not

obvious what sort of ionospheric altitude change is to be expected within this region, especially during storm time conditions. A difference of 50 km between the northern and the southern portions of images may be a relatively large change within a horizontal distance of about 1,200 km. We do a similar analysis applying a difference of 25 km in emission heights to the northern and southern portions of the observed images to see if similar results are obtained with a smaller altitude variation. This altitude variation is similar to the variation shown in the SAMI2 outputs in Figure 3. In Figure 6, the northern portion is unwrapped at 275 km and the southern portion is unwrapped at 250 km. For this mapping, the image is split at 9.7°N, the approximate location where the EPB is no longer N-S aligned and is tilting to the west. As with Figure 5, the split is at a constant latitude and not a constant zenith angle. Since this split is north of zenith, a small region of 0.1° of latitude is duplicated, rather than obfuscated. This does not impact our results. The projection of the northern portion of the image to the Southern Hemisphere is no longer completely outside the FoV of the imager; it overlaps with a small region. From Figure 1 we can see that the EPBs in the overlapped region are still north-south aligned like those near the center of the FoV. The projected portion of the image lines up well with the southern portion of the image. Figure 6 shows that even a variation of 25 km across the FoV of the image is enough to explain the hemispheric asymmetry, and if there is a variation of 50 km, the asymmetry would be even more pronounced.

4. Experimental Evidence for the Proposed Hypothesis

In the previous section we showed that it is reasonable to expect some variation in airglow altitude throughout the night and at different latitudes on the night of observation. In this section we discuss evidence for variation in airglow altitude with latitude and discuss the impact this variation has on the images.

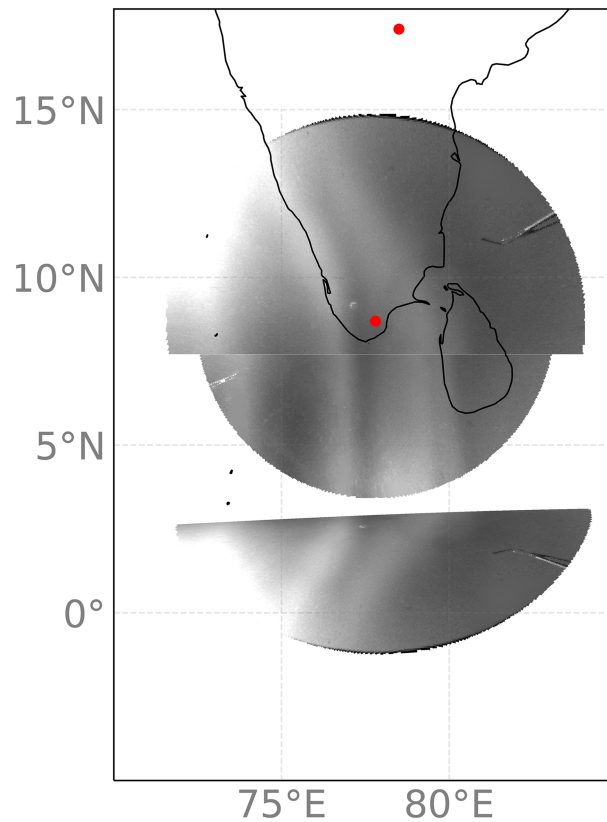


Figure 5. An image from the Tirunelveli ASI on 17 March 2015 at 17:06 UT, the same time as Figure 1. Instead of being unwrapped at a constant altitude, like in Figure 1, the northern portion of the image is unwrapped at 300 km and the southern portion of the image is unwrapped at 250 km. Additionally, the northern portion of the image is traced along magnetic field lines and is projected into the Southern Hemisphere at 250 km.

As mentioned before, we use measurements made by two ionosondes over Tirunelveli and Hyderabad to investigate ionospheric height variations in the Indian sector on the night of observation. We focus on the virtual heights of reflections with the aim of studying the bottomside height variation. However, over Hyderabad, the F region traces were scarcely present between 14:10 and 17:50 UT. The lack of F region traces over Hyderabad is also noted in Ramsingh et al. (2015). It may be noted that this time coincides with the time of observation of asymmetry in EPBs seen in airglow images. We believe that the lack of traces might be due to some geophysical process associated with storm time ionospheric electrodynamics. Investigating the cause of poor back reflections in this period is not in the scope of the current work. Nevertheless, in this duration, there were some ionograms with reflections around 7 MHz at 15:20, 16:00, 16:10, and 16:30 UT at Hyderabad. Over Tirunelveli, ionogram traces were present during the whole duration. Since traces over Hyderabad were available only between 6 and 8 MHz frequencies, we investigate possible height variation trends in the ionosphere during the time of observation of asymmetric EPBs using 7 MHz reflection heights over both locations.

In Figure 7, we show the virtual heights of the 7 MHz reflection measured by the ionosondes at Tirunelveli and Hyderabad between 10 and 22 UT on 17 March 2015. The dots and squares show the measured virtual heights, and the lines are spline interpolations through the data. The virtual height is not the actual height from where the reflection occurs. As the signal passes through the ionosphere, there is a change in the group velocity as it passes through changing electron densities. This means that the virtual height is slightly higher than the actual height. This difference does not impact the interpretation of the results. While there is data gap over Hyderabad as mentioned before, the spline interpolation appears to capture the variations reasonably, though it may not be entirely accurate. The alternate crests and troughs in the data points over Hyderabad indicate probable signatures of a large-scale traveling ionospheric disturbance (LSTID) that might have been generated by the geomagnetic disturbance. LSTIDs are the ionospheric signatures of atmospheric gravity waves with horizontal wavelengths greater than a few 100 km propagating

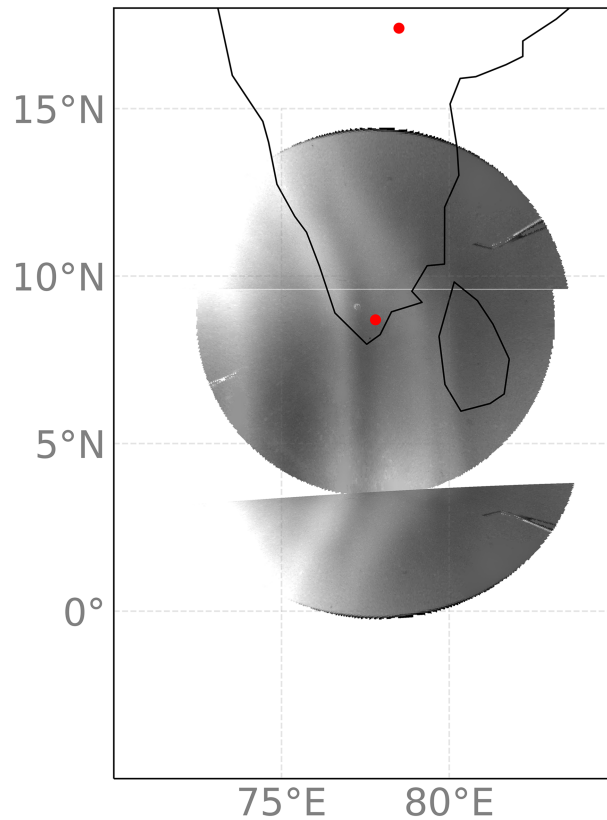


Figure 6. The same as Figure 5 except that the northern portion of the image is unwrapped at 275 km.

in the thermosphere. Large horizontal scale sizes correspond to time periods of a few hours. Quite often, such LSTIDs are generated in the high-latitude regions as a result of geomagnetic disturbances (Hunsucker, 1982; Oyama & Watkins, 2012). Once generated, they typically move toward the equatorial latitudes and at times reveal transhemispheric propagation as well (Ding et al., 2008). Observation of alternating crests and troughs is a typical indication of the existence of wave signatures like TIDs. It may be noted that the

continuity of the TID in this case is captured in the spline interpolation between regions where data are present and in the regions where data points are scarce. Therefore, it can be used to infer the overall trend in the data. The period of the TID appears to be between 2 and 3 hr from Figure 7. Earlier, Ramsingh et al. (2015) observed TID signatures with quasi 2 hr periodicity in the later part of the night. This further strengthens our confidence in the results of the spline interpolation in this case, which appear to capture the signature of the TID features for a longer duration than was identified in the earlier work. TIDs may be the reason for the variation of the ionospheric altitude that is responsible for the airglow altitude variation. Geomagnetic storms can produce both disturbance winds and TIDs, both of which are possible explanations for the ionospheric variation.

At Tirunelveli the ionosphere seems to be moving in the typical manner. After 12:00 UT the virtual height increases as a result of the PRE. There are no other major features visible in the behavior of the 7 MHz virtual height at Tirunelveli. In contrast, the 7 MHz virtual height at Hyderabad is more complex. Starting around 08:00 UT, the virtual height at 7 MHz oscillates up and down for about 13 hr, likely due to TIDs generated from the ongoing magnetic storm. While the study of the TIDs is not the aim of this work, we would like to point to the importance of the TIDs that

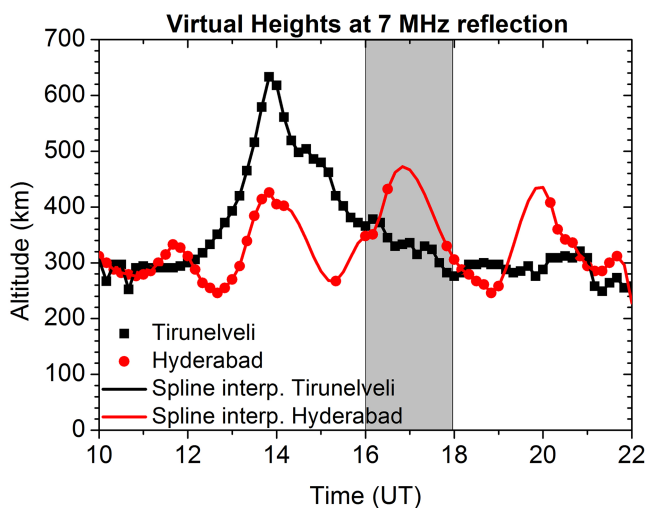


Figure 7. Virtual heights of the 7 MHz reflection point from ionosondes in Tirunelveli and Hyderabad. The lines between the points are spline interpolations. The gray shaded region from 16:00 to 18:00 UT is the time when hemispheric asymmetry is observed in the images.

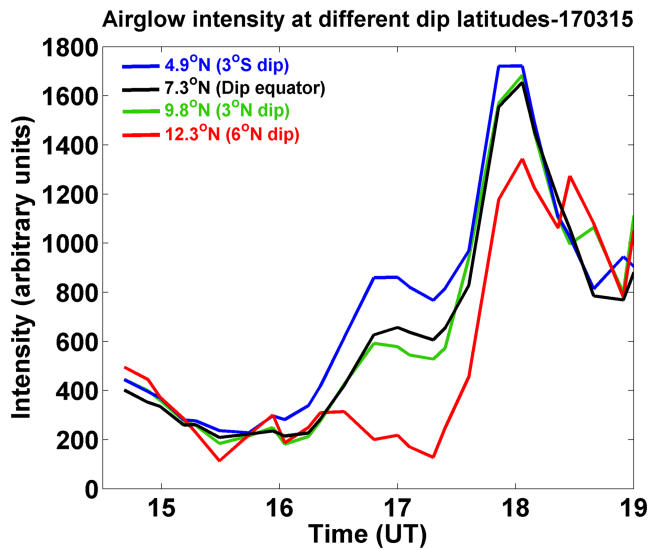


Figure 8. Intensity of airglow emission at various latitudes throughout the night from the Tirunelveli ASI. The different colored lines show different geographic (and geomagnetic) latitudes. The intensity profile is the mean extracted over a width of 21 km in the north-south direction centered on the chosen dip latitude and are from ± 400 km in the east-west direction.

are revealed clearly in Hyderabad data. The lack of oscillations at Tirunelveli may be due to the following factors. Being very close to the dip equator, the magnetic field lines are almost horizontal over Tirunelveli. As already mentioned, the TIDs are an ionospheric manifestation of gravity waves propagating in the neutral thermosphere. At F region heights, the neutral collisions can move the plasma mainly along the geomagnetic field lines and hence a tilted field line is more favorable for gravity wave associated perturbation to move the plasma up and down. Therefore, over Hyderabad where the magnetic inclination is 23.2° , the waves are more likely to be visible in the ionosphere compared to Tirunelveli where the inclination is only 3.3° . We are not able to determine what latitude these potential TIDs extend to, and they may be responsible for the variation in airglow altitude. Another reason for lack of prominent TID signatures over Tirunelveli is that the equatorial ionosphere responds to the zonal electric field fluctuations significantly. For example, it may be seen from Figure 7 that between 12 and 14 UT, the ionospheric height variation is dominated by a strong eastward electric field.

The gray shaded region shows the time when the hemispheric asymmetry in the airglow depletions is observed. During this time, data are mostly unavailable at Hyderabad but there are three data points where the reflection point at Hyderabad is higher than that at Tirunelveli. Additionally, data show that before the observation of hemispheric asymmetry, the ionosphere at Hyderabad started rising up. It is worth noting that the asymmetry is not observed for EPBs recorded after 18:00 UT. The higher altitude of reflection at Hyderabad supports the proposal that airglow altitude is higher in the northern half of the image. If the ionosphere is at higher altitude, then the airglow layer will also be at higher altitude. At the same time, a reduction in intensity will be expected if the thermospheric densities do not vary concurrently.

With the help of mean intensities in different latitudinal regions of the airglow images, we can check whether any relative reduction in intensity is noticed in the northern portions of images compared to the dip equatorial and Southern Hemispheric regions. Figure 8 shows the mean intensities extracted from the airglow images from 4.9°N , 7.3°N , 9.8°N , and 12.3°N latitude regions. These latitudes are selected because they correspond to 3°S , 0° , 3°N , and 6°N dip latitudes in the longitude of Tirunelveli. To construct this plot, first, we have selected individual east-west (EW) intensity profiles of 21 km width centered at a particular geographic latitude within zonal distance of ± 400 km from the longitude of Tirunelveli. All the pixel intensities within this cross section are averaged to obtain the mean intensity for the chosen latitude at a particular time. Though EPBs were present within most of the images on 17 March 2015, being linear features with similar width, their contribution to mean intensities should approximately be equal in all the four cross sections. Therefore, the mean intensities represent respective background OI 630 nm intensities at the corresponding latitudes. It can be clearly observed from Figure 8 that background intensities were comparable at all the latitudes before 16 UT and after 18:30 UT. Between 16 and 18:30 UT, intensity was lowest at 12.3°N latitude, while it was highest at 4.9°N latitude. It is interesting to observe from Figure 7 that the virtual height at 7 MHz over Tirunelveli and Hyderabad was comparable at 16:00 and 18:30 UT. In between 16 and 18:30 UT, virtual height at Hyderabad was higher than that at Tirunelveli. Therefore, the airglow emission intensity variation appears to be consistent with the higher ionospheric altitudes observed over Hyderabad relative to Tirunelveli. Thus, credible evidence is shown for a possible increase in the airglow altitude from the equatorial region to the northern latitudes around the time of observation of asymmetry in EPB features. This airglow altitude variation can explain the observed EPB asymmetry since a constant airglow layer altitude was assumed during image analysis in Sau et al. (2017).

5. Conclusions

Sau et al. (2017) showed an unusual observation where an asymmetry in the tilt of airglow depletions associated with ESF was observed. In this paper we show that this asymmetry does not contradict the field-aligned nature of ESF and can be explained by a nonuniform airglow layer altitude within the FoV of the imager.

SAMI2 is used to show that a variation in the airglow altitude with latitude within the FoV of the imager is possible during a geomagnetic storm. Analysis using various airglow altitudes and then tracing portions of the image along magnetic field lines and projecting them into the opposite hemisphere shows that this variation in airglow altitude can account for this asymmetry. Measurements from the ionosondes at Hyderabad and Tirunelveli indicate that the ionospheric altitudes over Hyderabad are higher by more than 50 km than Tirunelveli which provides evidence for a higher airglow altitude north of the dip equator. Airglow intensities extracted from different portions of images also support the possibility of an increasing altitude to the north of the magnetic equator. This variation in ionospheric altitude may be due to meridional winds associated with the geomagnetic storm or may be due to the presence of LSTIDS, whose presence can be inferred from Hyderabad measurements as well. From all these consistent results, we believe that a variation in the airglow altitude can explain the hemispheric asymmetry and the modeling and observational evidence indicates that a variation in the airglow altitude is likely occurring on this night.

Acknowledgments

This work was done while D. H. held an NRC Research Associateship award at the U.S. Naval Research Laboratory. D. H.'s work is supported by the Office of Naval Research. The work of S. S. and S. G. was supported by the Department of Science and Technology, Government of India through IIG. We acknowledge Mr. B. Suneel Kumar, in-Charge, TIFR Balloon Launch Facility, Hyderabad, for providing the Hyderabad CADI data under a joint MOU with IIG. VLN acknowledges the support from Research Council of Norway through the grant NFR 275503. Data sets used for this research are available in this reference: Hickey et al. (2020). The IRI model code in Fortran is available from the IRI homepage (irmodel.org), NRLMSISE-00 is available online (<https://ccmc.gsfc.nasa.gov/pub/modelweb/atmospheric/msis/nrlmsise00/>). SAMI2 is available to download online (<https://www.nrl.navy.mil/ppd/branches/6790/sami2/downloads>). The authors thank Dr. S. Sripathi, IIG, Navi Mumbai, for his useful comments on this work.

References

- Abalde, J. R., Fagundes, P. R., Sahai, Y., Pillat, V. G., Pimenta, A. A., & Bittencourt, J. A. (2004). Height-resolved ionospheric drifts at low latitudes from simultaneous OI 777.4 nm and OI 630.0 nm imaging observations. *Journal of Geophysical Research*, *109*, A11308. <https://doi.org/10.1029/2004JA010560>
- Abdu, M. A., Sobral, J. H. A., & Batista, I. S. (2000). Equatorial spread F statistics in the American longitudes: Some problems relevant to ESF description in the IRI scheme. *Advances in Space Research*, *25*(1), 113–124.
- Bilitza, D., Altadill, D., Truhlik, V., Shubin, V., Galkin, I., Reinisch, B., & Huang, X. (2017). International reference ionosphere 2016: From ionospheric climate to real-time weather predictions. *Space Weather*, *15*, 418–429. <https://doi.org/10.1002/2016SW001593>
- Colerico, M. J., Mendillo, M., Fesen, C. G., & Meriwether, J. (2006). Comparative investigations of equatorial electrodynamic and low-to-mid latitude coupling of the thermosphere-ionosphere system. *Annales Geophysicae*, *24*(2), 503–513.
- Ding, F., Wan, W., Liu, L., Afraimovich, E. L., Voeykov, S. V., & Perevalova, N. P. (2008). A statistical study of large-scale traveling ionospheric disturbances observed by GPS TEC during major magnetic storms over the years 2003–2005. *Journal of Geophysical Research*, *113*, A00A01. <https://doi.org/10.1029/2008JA013037>
- Emmert, J. T., Richmond, A. D., & Drob, D. P. (2010). A computationally compact representation of magnetic-apex and quasi-dipole coordinates with smooth base vectors. *Journal of Geophysical Research*, *115*, A08322. <https://doi.org/10.1029/2010JA015326>
- Farley Jr., D. T. (1960). A theory of electrostatic fields in the ionosphere at nonpolar geomagnetic latitudes. *Journal of Geophysical Research*, *65*(3), 869–877. <https://doi.org/10.1029/JZ065i003p00869>
- Hedin, A. E., Salah, J. E., Evans, J. V., Reber, C. A., Newton, G. P., Spencer, N. W., et al. (1977). A global thermospheric model based on mass spectrometer and incoherent scatter data MSIS, 1. N_2 density and temperature. *Journal of Geophysical Research*, *82*(16), 2139–2147. <https://doi.org/10.1029/JA082i016p02139>
- Hickey, D. A., Martinis, C. R., Mendillo, M., Baumgardner, J., Wroten, J., & Milla, M. (2018). Simultaneous 6300 Å airglow and radar observations of ionospheric irregularities and dynamics at the geomagnetic equator. *Annales Geophysicae*, *36*, 473–487.
- Hickey, D. A., Sau, S., Naryanan, L. V., & Gurubaran, S. (2020). Data for “a possible explanation of interhemispheric asymmetry of equatorial plasma bubbles in airglow images”. Zenodo, <https://doi.org/10.5281/zenodo.3688797>
- Huba, J. D., Joyce, G., & Fedder, J. A. (2000). Sami2 is Another Model of the Ionosphere (SAMI2): A new low-latitude ionosphere model. *Journal of Geophysical Research*, *105*(A10), 23035–23053.
- Hunsucker, R. D. (1982). Atmospheric gravity waves generated in the high-latitude ionosphere: A review. *Reviews of Geophysics*, *20*(2), 293–315. <https://doi.org/10.1029/RG020i002p00293>
- Hysell, D. L., & Burcham, J. D. (2002). Long term studies of equatorial spread F using the JULIA radar at Jicamarca. *Journal of Atmospheric and Solar-Terrestrial Physics*, *64*(12), 1531–1543.
- Kelley, M. C., Kotsikopoulos, D., Beach, T., Hysell, D., & Musman, S. (1996). Simultaneous global positioning system and radar observations of equatorial spread F at Kwajalein. *Journal of Geophysical Research*, *101*(A2), 2333–2341. <https://doi.org/10.1029/95JA02025>
- Martinis, C., Eccles, J. V., Baumgardner, J., Manzano, J., & Mendillo, M. (2003). Latitude dependence of zonal plasma drifts obtained from dual-site airglow observations. *Journal of Geophysical Research*, *108*(A3), 1129. <https://doi.org/10.1029/2002JA009462>
- Martinis, C. R., Mendillo, M. J., & Aarons, J. (2005). Toward a synthesis of equatorial spread F onset and suppression during geomagnetic storms. *Journal of Geophysical Research*, *110*, A07306. <https://doi.org/10.1029/2003JA010362>
- Mendillo, M., & Baumgardner, J. (1982). Airglow characteristics of equatorial plasma depletions. *Journal of Geophysical Research*, *87*(A9), 7641–7652.
- Narayanan, V. L., Sau, S., Gurubaran, S., Shiokawa, K., Balan, N., Emperumal, K., & Sripathi, S. (2014). A statistical study of satellite traces and evolution of equatorial spread F. *Earth, Planets and Space*, *66*(1), 160. <https://doi.org/10.1186/s40623-014-0160-4>
- Otsuka, Y., Shiokawa, K., Ogawa, T., & Wilkinson, P. (2002). Geomagnetic conjugate observations of equatorial airglow depletions. *Geophysical Research Letters*, *29*(15), 1753. <https://doi.org/10.1029/2002GL015347>
- Oyama, S., & Watkins, B. J. (2012). Generation of atmospheric gravity waves in the polar thermosphere in response to auroral activity. *Space Science Reviews*, *168*, 463–473.
- Picone, J. M., Hedin, A. E., Drob, D. P., & Aikin, A. C. (2002). NRLMSISE-00 empirical model of the atmosphere: Statistical comparisons and scientific issues. *Journal of Geophysical Research*, *107*(A12), 1468.
- Rama Rao, P. V. S., Niranjan, K., Prasad, D. S. V. D., Gopi Krishna, S., & Uma, G. (2006). On the validity of the ionospheric pierce point (IPP) altitude of 350 km in the Indian equatorial and low-latitude sector. *Annales Geophysicae*, *24*(8), 2159–2168.
- Ramsingh, Sripathi, S., Sreekumar, S., Banola, S., Emperumal, K., Tiwari, P., & Kumar, B. S. (2015). Low-latitude ionosphere response to super geomagnetic storm of 17/18 March 2015: Results from a chain of ground-based observations over Indian sector. *Journal of Geophysical Research: Space Physics*, *120*, 10,864–10,882. <https://doi.org/10.1002/2015JA021509>
- Richmond, A. D. (1995). Ionospheric electrodynamic using magnetic apex coordinates. *Journal of geomagnetism and geoelectricity*, *47*(2), 191–212.
- Sau, S., Narayanan, V. L., Gurubaran, S., & Emperumal, K. (2018). Study of wave signatures observed in thermospheric airglow imaging over the dip equatorial region. *Advances in Space Research*, *62*(7), 1762–1774.

- Sau, S., Narayanan, V. L., Gurubaran, S., Ghodpage, R. N., & Patil, P. T. (2017). First observation of interhemispheric asymmetry in the EPBS during the St. Patrick's Day geomagnetic storm of 2015. *Journal of Geophysical Research: Space Physics*, *122*, 6679–6688. <https://doi.org/10.1002/2017JA024213>
- Sobral, J. Z., Takahashi, H., Abdu, M., Muralikrishna, P., Sahai, Y., J. Zamlutti, C., et al. (1993). Determination of the quenching rate of the $O(^1D)$ by $O(^3P)$ from rocket-borne optical (630 nm) and electron density data. *Journal of Geophysical Research*, *98*, 7791–7798.
- Tulasi Ram, S., Rama Rao, P. V. S., Prasad, D. S. V. D., Niranjana, K., Gopi Krishna, S., Sridharan, R., & Ravindran, S. (2008). Local time dependent response of postsunset ESF during geomagnetic storms. *Journal of Geophysical Research*, *113*, A07310. <https://doi.org/10.1029/2007JA012922>
- van der Meeren, C., Burrell, A. G., & Laundal, K. M. (2018). apexy: Apexy version 1.0.3.
- Weber, E. J., Aarons, J., & Johnson, A. L. (1983). Conjugate studies of an isolated equatorial irregularity region. *Journal of Geophysical Research*, *88*(A4), 3175–3180.
- Weber, E. J., Buchau, J., Eather, R. H., & Mende, S. B. (1978). North-south aligned equatorial airglow depletions. *Journal of Geophysical Research*, *83*(A2), 712–716.
- Weber, E. J., Buchau, J., & Moore, J. G. (1980). Airborne studies of equatorial F layer ionospheric irregularities. *Journal of Geophysical Research*, *85*(A9), 4631–4641.